RESEARCH ARTICLE

NANO · MICRO small
www.small-journal.com

Photo-Induced Geometry and Polarity Gradients in Covalent Organic Frameworks Enabling Fast and Durable Molecular Separations

*Congcong Yin, Lin Liu, Zhe Zhang, Ya Du, and Yong Wang**

Azobenzene, which activates its geometric and chemical structure under light stimulation enables noninvasive control of mass transport in many processes including membrane separations. However, producing azobenzene-decorated channels that have precise size tunability and favorable pore wall chemistry allowing fast and durable permeation to solvent molecules, remains a great challenge. Herein, an advanced membrane that comprises geometry and polarity gradients within covalent organic framework (COF) nanochannels utilizing photoisomerization of azobenzene groups is reported. Such functional variations afford reduced interfacial transfer resistance and enhanced solvent-philic pore channels, thus creating a fast solvent transport pathway without compromising selectivity. Moreover, the membrane sets up a densely covered defense layer to prevent foulant adhesion and the accumulation of cake layer, contributing to enhanced antifouling resistance to organic foulants, and a high recovery rate of solvent permeance. More importantly, the solvent permeance displays a negligible decline throughout the long-term filtration for over 40 days. This work reports the geometry and polarity gradients in COF channels induced by the conformation change of branched azobenzene groups and demonstrates the strong capability of this conformation change in realizing fast and durable molecular separations.

1. Introduction

Azobenzene and its derivates are archetypal molecules that play a central role in fundamental and applied studies thanks to their distinctive advantages, such as robust photoswitching behavior, straightforward and versatile design, and rich chemistry.[1–3] The isomerization of azobenzene groups has been used as a synthetic tool to precisely and reversibly control the chemical and mechanical properties of various materials. In particular, the conformation of azobenzene can be switched from the stretched *trans* form to the compact *cis* form by means of light, whereas the reverse interconversion can occur by light or thermal energy.[4–6] The azobenzene group in the *trans* conformation has a length of 9.0 Å while its *cis* counterpart has a length of 5.5 Å. Besides, azobenzene can isomerize from the nonpolar form to the nonplanar form with a dipole moment of 3 Debye, leading to a remarkable polarity enhancement accompanied by the size change. Due to these behaviors, the incorporation of azobenzene units has enabled the construction of photoresponsive materials with smart properties that can be externally manipulated by light with unprecedented temporal and spatial control.[7–9] Particularly, notable advances involving azobenzene have emerged in tunable mass transport upon simple light irradiation, thus making them the preferred choice for task-specific demands.[10,11]

To realize precise control over mass transport, it is imperative to arrange the azobenzene units into well-ordered nanochannels. The regular structure could strategically ensure the homogeneous distribution of azobenzene groups and the accuracy of pore size change, thus upgrading the responsive efficiency.[12–14] In this regard, Wang and coworkers constructed photoresponsive nanochannels by confining azobenzene groups into metal-organic frameworks (MOFs).[15] Upon UV exposure, trans-state azobenzene was transformed into the *cis* structure, resulting in an unusual open-to-closed switching of MOF pores at the Angstrom scale. For a deep understanding of the azobenzene isomerization within MOF channels, Woll and coworkers combined experimental studies and theoretical calculations to investigate the photo-induced structural transformation.[16] The result implies that a well-ordered framework is highly required during the isomerization process, which would provide sufficient space to enable trans-cis switching. However, the chelation between metal sites and azobenzene groups would

C. Yin, Y. Wang
School of Energy and Environment
Southeast University
Nanjing, Jiangsu 210096, P. R. China
E-mail: yongwang@seu.edu.cn
C. Yin, Z. Zhang, Y. Wang
State Key Laboratory of Materials-Oriented Chemical Engineering
College of Chemical Engineering
Nanjing Tech University
Nanjing, Jiangsu 211816, P. R. China
L. Liu, Y. Du
Institute of Advanced Synthesis
School of Chemistry and Molecular Engineering
Nanjing Tech University
Nanjing, Jiangsu 211816, P. R. China

The ORCID identification number(s) for the author(s) of this article can be found under https://doi.org/10.1002/smll.202309329

DOI: 10.1002/smll.202309329

inevitability lead to the dull torsion of azobenzene, thus compromising the responsive efficiency. Alternatively, covalent organic frameworks (COFs) with pure organic skeletons and extraordinary chemical stability have grown into the emerging photoresponsive platform.[17–19] 2D COFs are eminent over their ultralow density, permanent porosity, structural diversity, and high stability in diverse solvents.[20–22] In the case of azobenzene modification and isomerization, those distinctive superiorities may offer great compatibility and enhanced photoconversion efficiency. For instance, Zhu and coworkers pioneered the exploration of azobenzene units as building blocks to construct azo-containing COFs, in which the structural regularity can be greatly maintained after photoisomerization.[23] Trabolsi and coworkers designed a light-responsive COF with pendant azobenzene groups that can precisely regulate the pore size for several cycles, resulting in a controlled release of guest molecules.[24] In spite of these important progresses, current studies mainly focus on insoluble powders, restricting their widespread applications. To realize accurate control over the mass transport in COF channels, several efforts have been made to fabricate continuous photoresponsive COF membranes.[25,26] Quantitative conversion of azobenzene groups could offer a more progressive way of tailoring the geometric and chemical structure. In addition, the shielding effect arising from the isomerization process significantly affects the mass transport behavior, enabling on-demand separations. Therefore, fine control over the azobenzene groups within COF membranes is expected to markedly advance the separation processes, which, however, has so far remained unexplored.

There are two major obstacles in fabricating tailor-made COF membranes with elaborate mass transport functions. The first is the geometric structure of pore channels after light exposure. In the isomerization of azobenzene groups, often the pore size is altered at two states. We expect that if the pore conformation occurs in a suitable way, there might be a chance to favor fast mass transport. Therefore, the demand to develop unique pore structures, for example, asymmetric membranes with gradient pore structures remains.[27] The second is the manipulation of interactions between solvent molecules and pore walls, which is of vital significance to mass transport efficiency. Precise control of the interactions may create a favorable and on-demand pore environment for fast solvent transport.[28] Meanwhile, strengthened interactions could promote solvent molecules attaching to the pore walls, which forms a protective layer and helps to prevent solutes from adhesion but allows solvents to pass through. However, this method is yet limited, as the azobenzene groups rapidly transform from the trans to cis state under UV exposure, making it difficult to precisely regulate the pore environment. To this end, should pore conformation and environment occur in a favorable way, the COF membranes would be expected to meet the demand for efficient mass transport.

Herein, we engineer both geometry and polarity gradients along the COF pore channels to boost the solvent permeation and fouling resistance. Azobenzene-branched hydrazide linkers are reacted with aldehydes to create functional side chains within nanochannels. Via interfacial polymerization, a continuous COF selective layer is formed on the porous substrate, which exhibits a high crystallinity and structural rigidity. By tuning the photo exposure time, pore size and polarity gradients progressively occurring from surface to interior are simultaneously realized (**Figure 1a**). On the one hand, the isomerization of azobenzene groups enlarges the pore size of the membrane upper layer and thus ensures superior solvent permeation (Figure 1b). On the other hand, the polarity of the membrane surface is greatly enhanced, leading to a compact defense layer through the dipole-dipole interaction, effectively preventing nonspecific pollutant adsorption (Figure 1c). Such specifically engineered channels enable fast and durable separation processes, which are highly desired in practical applications.

2. Results and Discussion

2.1. Synthesis of Azobenzene-Branched COF Membranes

The pore size and polarity gradients are engineered based on the regulation of azobenzene groups aligned on the pore walls. We selected Azo-TbTh with high-density azobenzene groups as the representative photoresponsive COF for investigations (**Figure 2a**). Azo-TbTh membranes were synthesized by covalently linking 1,3,5-triformylbenzene (Tb) and 2, 5-(azobenzeneoxy)-terephthalohydrazide (Azo-Th) on the polyacrylonitrile (PAN) substrate via interfacial polymerization (Figure 2b). Scanning electron microscopy (SEM) revealed defect-free, continuous COF layers formed on the substrate over the synthetic course of 3 days (Figure S1, Supporting Information). Besides, the cross-sectional morphology shown in Figure S2 (Supporting Information) reveals that the thickness of the Azo-TbTh layers can be finely tuned by varying the synthesis duration. Longer synthesis duration generally produces thicker Azo-TbTh layers. The thickness was increased from 50 to 135 nm when the synthesis was prolonged from 3 to 9 days (Figure S3, Supporting Information). To obtain more insights into the structure of the synthesized Azo-TbTh, we dissolved away the PAN substrate to release the Azo-TbTh layer. With the removal of PAN, the Azo-TbTh layer synthesized with a duration of 5 days was estimated to be ≈125 nm in thickness by atomic force microscopy (AFM), which is in agreement with the SEM observation (Figure S4, Supporting Information). The chemical structure of the resulting Azo-TbTh was confirmed by the Fourier transform infrared spectroscopy (FTIR) analysis as a new peak at 1673 cm^{-1} assigned to C═N stretching appeared (Figure S5, Supporting Information).[29]

We shed UV light on the Azo-TbTh layers to precisely and continuously regulate their pore environment. Analysis of the *trans-cis* photoisomerization process was first performed on Azo-TbTh dispersed in DMF. Figure 2c shows that the pristine Azo-TbTh before UV exposure possesses two distinct bands at 320 and 455 nm, indicative of π-π^* and n-π^* transitions of azobenzene groups. Upon UV exposure, the intensity of the absorption band at 320 nm decreased instantly and remained unaltered after exposure for 10 min, while the intensity of the absorption band at 455 nm slightly increased. Notably, the yield of the trans-cis isomerization was determined to be 68% by comparing the intensity of the absorption band at 320 nm before and after UV exposure, which is comparable or even higher than that of previously reported photoresponsive COFs.[24,26] This should be mainly attributed to the branched azobenzene groups establishing high-density photoresponsive sites on directionally aligned nanochannels. For convenience, Azo-TbTh before and after UV exposure to induce the *trans-cis* isomerization is termed as Azo-TbTh-*trans*

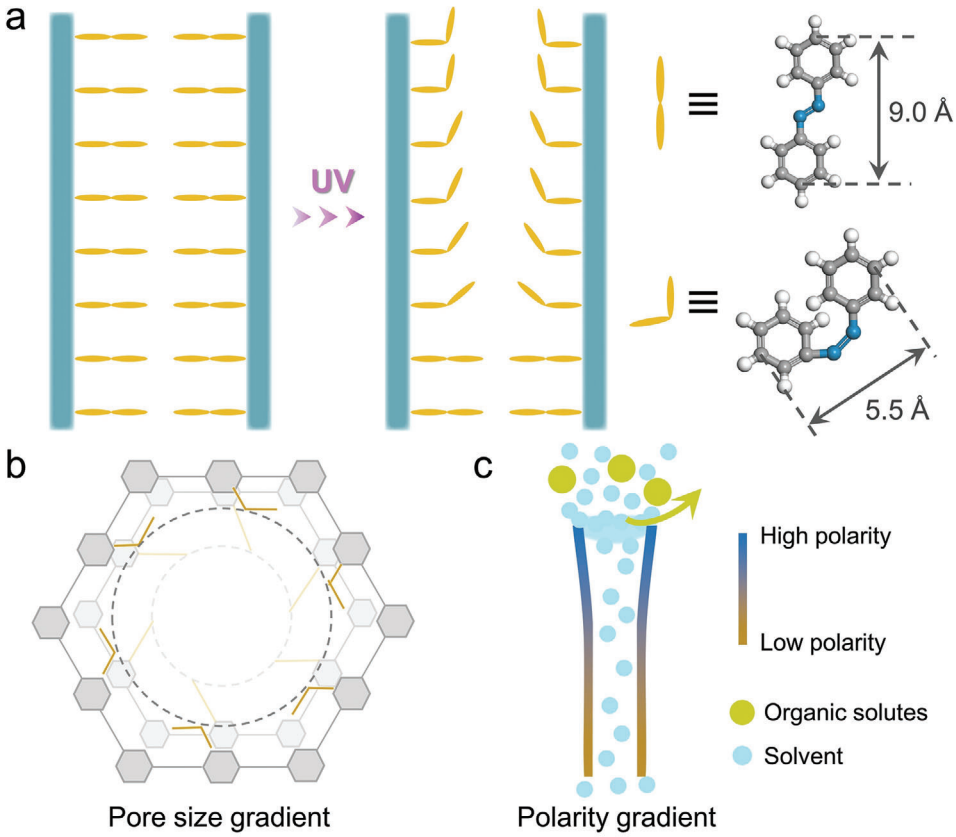

Figure 1. Schematic illustration of the azobenzene-branched COF membrane. a) The isomerization of azobenzene groups branched to the COF channels subjected to UV exposure. b) Engineering pore size gradient in COF by controlling the conformation of azobenzene groups. c) Polarity gradient across the COF channels for the formation of a defense layer and against fouling.

and Azo-TbTh-*cis*, respectively although azobenzene groups are present in both states in either case. We then studied their structural stability under exposure to UV light. As demonstrated in Figure 2d, the Azo-TbTh film exhibits an intense peak at 3.4° and a minor peak at 6.8°, affiliating to (100) and (200) facets, respectively. The lattice modeling of Azo-TbTh was simulated using the Materials Studio, which outputs the probable structure of Azo-TbTh with the eclipsed stacking mode. Notably, the crystallinity of the Azo-TbTh layer was greatly maintained and not affected by the isomerization of branched azobenzene groups. Besides, the eclipsed stacking mode was not changed, ensuring the framework integrity during isomerization. At the same time, the Azo-TbTh membrane shows a similar morphology after UV exposure, further proving its stability (Figure S6, Supporting Information). Furthermore, the effects of UV exposure on the 3D structure and rigidity were investigated by AFM. After UV exposure, the average surface roughness (*Ra*) of the Azo-TbTh layer was slightly increased from 3.3 to 4.5 nm, which is ascribed to the nonplanar *cis* structure of azobenzene groups that affect the stacking interactions (Figure 2e).[24,26,30] In addition, peak force quantitative nanomechanical mapping (PFQNM) reveals that the Azo-TbTh layer still possesses a high Young's modulus of 3.2 GPa after UV exposure (Figure S7, Supporting Information). The high structural rigidity affords permanent pores, which are critical for fast and stable solvent permeation.

The gradient functionality of the Azo-TbTh membrane was studied using the XPS depth profile analysis. To obtain the elemental information at different depths, the released Azo-TbTh layer was transferred onto a silicon substrate, followed by Ar-ion etching (Figure S8, Supporting Information). Ar-ion etching and XPS scans were alternately performed from the top surface of the Azo-TbTh layer to the silicon substrate until Si 2p appeared. The etching speed is determined to be 5.2 nms^{-1}, and the elemental composition at different depths of the Azo-TbTh layer can be precisely detected by changing the etching time. As shown in Figure 2f and Figure S9 (Supporting Information), the peak area ratio of C-N (*cis*) to C-N (*trans*) gradually drops from 0.98 to 0.33 with increasing depth. It is notable that the dipole moment of the *cis* isomer is significantly higher than that of the trans isomer, causing an increase in the polarity and thus producing a more hydrophilic surface.[24,31] Therefore, the isomerization degree continuously changed from the surface to the interior, endowing the nanochannels in the Azo-TbTh layer gradually change polarity, which is, a chemical gradient as azobenzene groups in the cis and trans state exhibiting opposite hydrophilicity. To evaluate the effect of azobenzene isomerization on pore aperture, we performed N_2 sorption tests on Azo-TbTh membranes at 77 K, and their pore size distributions were obtained using the nonlocal density functional theory (NLDFT) (Figure S10, Supporting Information). For the Azo-TbTh-*trans* membrane, the pore size is calculated to be

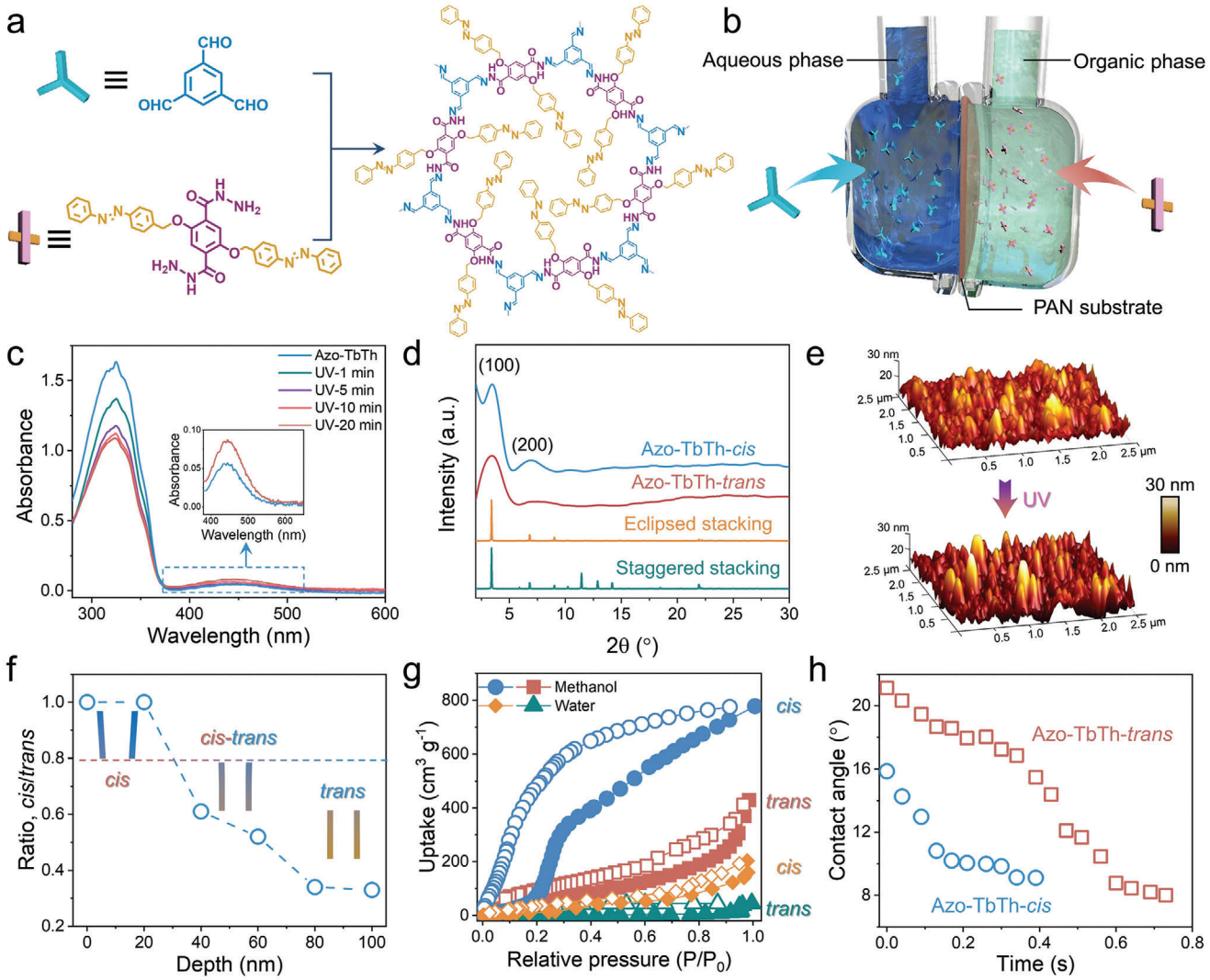

Figure 2. Structures and properties of the Azo-TbTh film before and after UV exposure. a) Schematic diagram for the reaction in the synthesis of Azo-TbTh. b) Schematic diagram for the interfacial polymerization of Azo-TbTh on PAN substrates. c) UV–Vis spectra of the Azo-TbTh layer exposed to 365 nm UV light for different durations. Inset are the zoomed UV–Vis spectra showing a new band appearing at 445 nm. d) Experimental and simulated XRD patterns of the Azo-TbTh films. e) The AFM surface morphologies. f) Peak area ratios of C-N (*cis*) to C-N (*trans*) of the Azo-TbTh film subjected to UV exposure for 40 min. g) Adsorption-desorption isotherms of the Azo-TbTh-*trans* layer tested in water (cyan) and methanol (red), and the Azo-TbTh-*cis* membrane tested in water (yellow) and methanol (blue). h) Dynamic methanol contact angles.

9.9 Å. After UV exposure, the pore size distribution peaks of Azo-TbTh-*cis* membrane are mainly focused at 10.2 and 12.1 Å, indicating the existence of two kinds of pores. This confirms the formation of gradient nanochannels, as the azobenzene groups with the *cis* form present a collapsed structure, leading to enlarged pore size in the upper layer of the Azo-TbTh-*cis* membrane. Furthermore, the water and methanol vapor uptake capacities were collected at 298 K to evaluate the solvent affinity of the Azo-TbTh layer (Figure 2g). The water vapor uptake of Azo-TbTh-trans is low even at high relative pressures (P/P_0>0.6), reflecting its hydrophobicity. Significantly, enhanced sorption capacity was observed for Azo-TbTh-*trans* when methanol was used as the adsorbate. After UV exposure, the capillary condensation zone was greatly broadened and vapor uptake was dramatically increased. This is because the azobenzene groups branched to the pore walls are mainly in the *cis* state. The *trans-cis* isomerization of the azobenzene enlarges the effective pore size on one hand and strengthens the polarity of the pore walls on the other, and the two factors both favor vapor molecules to access the pores. Notably, the methanol uptake of Azo-TbTh-*trans* is obviously higher than the water uptake of Azo-TbTh-*cis*, indicating that the pore wall-bearing azobenzene groups have a higher affinity to methanol molecules. To further evaluate the methanol affinity of the Azo-TbTh layer, we studied its wettability by contact angle analysis. As shown in Figure 2h, the initial contact angle is ≈21° and quickly decreases to 10° within 0.6 s, demonstrating a good methanol wettability. Upon UV exposure at 365 nm for 40 min, the contact angle falls down to 10° within 0.3 s, which indicates that the

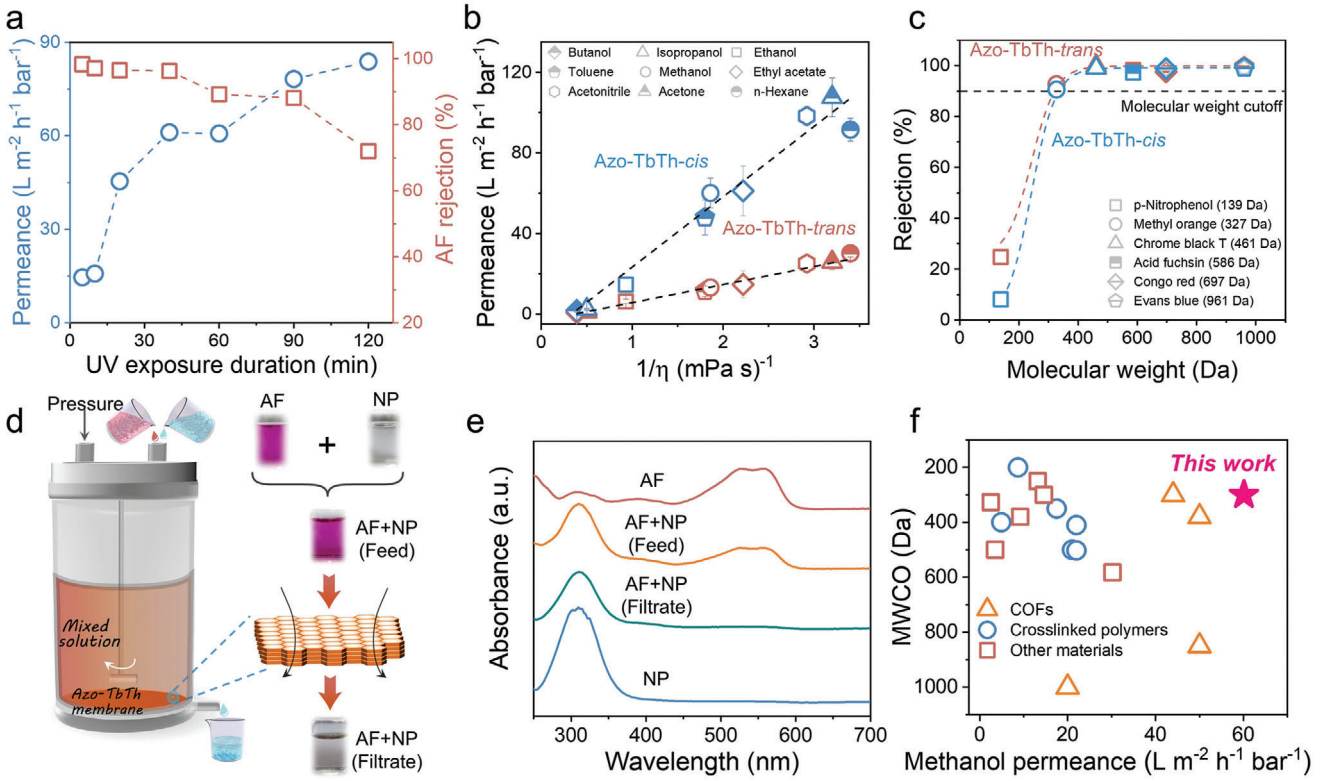

Figure 3. Separation performances of the Azo-TbTh membrane. a) Methanol permeance and AF rejection of the Azo-TbTh membrane subjected to UV exposure for various durations. b) Permeance of pure solvents with different viscosities. c) Rejection to solutes with different MWs. The sigmoidal curves were fitted with a Doseresp model. d) Schematic of the OSN process and selective separation of NP from a mixed solution of AF and NP. Photographs showing the AF and NP solution before and after filtration. e) UV–Vis spectra corresponding to the selective separation of NP from the mixture of AF and NP. f) Comparison of the OSN performance of our membrane and other membranes reported in the literature.

trans-cis isomerization induced by UV exposure accelerates the permeation of methanol through the Azo-TbTh layer.

2.2. Molecular Separation in Organic Solvents

The transport properties of the Azo-TbTh membranes were evaluated in terms of methanol permeance and acid fuchsin (AF) rejection. It can be seen from Figure S11 (Supporting Information) that the methanol permeation sharply declines with the extension of synthesis durations. This is due to the rising thickness of the Azo-TbTh layer which gives increased mass transfer resistance. Specifically, the Azo-TbTh membrane synthesized for 7 days exhibits the optimized performance with nearly maximized AF rejection of 98.1% and a methanol permeance of 13.2 L m^{-2} h^{-1} bar^{-1}. Then, we investigated the separation performance of this membrane subjected to UV exposure for various durations (**Figure** 3a). Generally, UV exposure significantly increases the permeance while moderately decreasing rejection, and longer UV exposure time leads to larger permeance and smaller rejection. Specifically, when the UV exposure duration is prolonged from 5 to 40 min, the permeance soars from 15 to 61 L m^{-2} h^{-1} bar^{-1} while the AF rejection is slightly decreased from 98% to 96%. This is because UV exposure enlarges the pore size of the upper Azo-TbTh layer. Therefore, we can conclude that the UV light functions as a remote controller to delicately tune the pore size and correspondingly the molecular separation properties of the Azo-TbTh membranes.

To gain deep insights into photoisomerization, we then tested the permeation of different solvents through the Azo-TbTh membranes (Figure 3b). The solvent permeance of the membrane before UV exposure exhibits a linear proportion to the inverse solvent viscosity, demonstrating the dominant role of solvent viscosity. This viscous flow behavior is mainly attributed to the rigid pore channels of the Azo-TbTh membrane, following the Hagen-Poiseuille equation.[32–34] Upon UV exposure for 40 min, a significant enhancement of the solvent permeance is observed, especially for polar solvents. It is notable that the membrane gives a high methanol permeance of 61 L m^{-2} h^{-1} bar^{-1}, which is 4 times higher than that of the membrane before UV exposure. This tremendous enhancement in permeance is attributed to enlarged pores and enhanced affinity of the pore wall to polar solvents as the azobenzene groups in the cis-state have higher affinity to polar molecules (Figure 2g).

Rejection tests were conducted in methanol using a variety of solutes with different molecular weights ranging from 139 to 961 Da. As shown in Figure 3c, the Azo-TbTh membrane before and after UV exposure shows similar rejection characterization with the MWCO of ≈320 Da. This is because UV exposure only enlarges the upper part of the Azo-TbTh pore channels while the

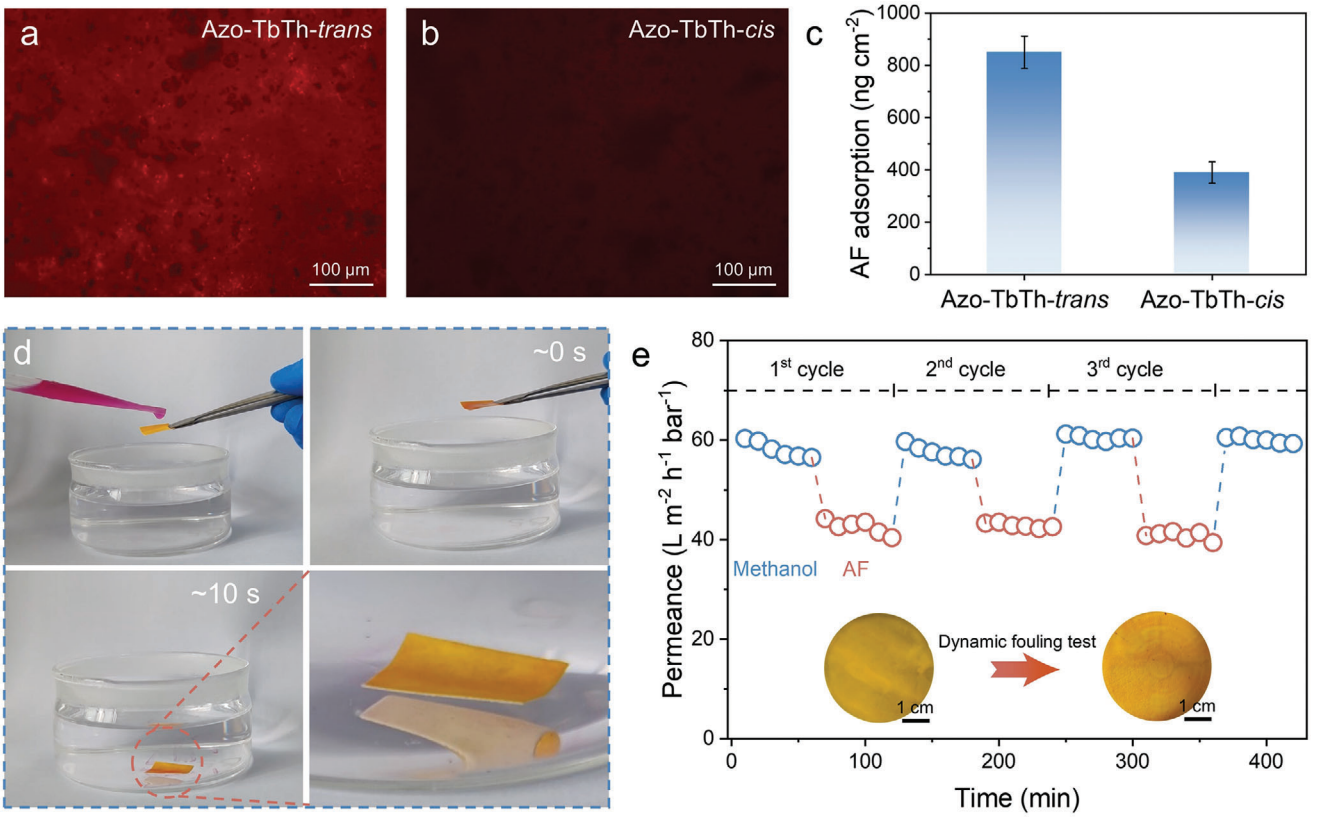

Figure 4. Antifouling performance of the Azo-TbTh membrane. Fluorescent images of the Azo-TbTh-*trans* a) and Azo-TbTh-*cis* b) membrane after AF adsorption test. c) Static AF adsorption capacity. d) Photographs of the self-cleaning characteristic of the Azo-TbTh-*cis* membrane after contact with AF. e) Permeance of the Azo-TbTh-*cis* membrane during alternate methanol and AF filtration. Insets represent the optical images of the Azo-TbTh-*cis* membrane before and after the test.

bottom part remains unchanged and determines the rejection. Molecules with MWs higher than 320 Da can be effectively rejected with rejection rates higher than 90%, while molecules with MWs lower than 200 Da can easily permeate through the pore channels with rejection rates less than 30%. Slightly higher rejection to *p*-Nitrophenol (NP) is observed for the Azo-TbTh membrane after UV exposure. Furthermore, a mixed molecular separation test was performed on the membrane after UV exposure using probe molecules of AF and NP (Figure 3d; Figure S12, Supporting Information). As shown in Figure 3e, the NP molecule with a smaller size (0.7 X 0.5 nm) can pass through the membrane easily, while AF with a larger size (1.2 X 1.1 nm) is completely blocked. Therefore, sharp selectivity between these molecular weight domains can be achieved, demonstrating the impressive sieving ability of this UV-exposed Azo-TbTh membrane.

To present a straightforward demonstration of the molecular separation, we carried out a comparison of methanol permeance versus the reciprocal MWCO for the UV-exposed Azo-TbTh membrane, along with data for the state-of-the-art membranes (Table S1, Supporting Information). As demonstrated in Figure 3f, the UV-exposed Azo-TbTh membrane shows a record-high methanol permeance that is ≈2–4 times higher than other membranes with a comparable MWCO based on COFs or crosslinked polymers. It indicates that photo-isomerization could engineer pore size and polarity gradients along the channels, significantly boosting solvent permeation and molecular separation capability.

2.3. Photo-Induced Fouling Resistance

The Azo-TbTh-*cis* membrane is expected to exhibit enhanced fouling resistance because of the stronger polarity of azobenzene groups in the *cis* state branched to the pore walls. Static molecular adsorption tests were first performed using AF as the model foulant to study its anti-fouling behavior. The membrane was kept in the methanolic solution of AF for 24 h and qualitatively analyzed by the fluorescence microscope. For the pristine Azo-TbTh membrane before UV exposure, obvious fluorescence spots originating from the absorbed AF molecules are observed (**Figure** 4a). By contrast, the membrane subjected to UV exposure shows a non-fluorescent surface, indicative of its strong resistance to AF adsorption (Figure 4b). Besides, the AF adsorption of the Azo-TbTh membrane is significantly reduced from 850 ng cm^{-1} before UV exposure to 390 ng cm^{-1} after UV exposure, further suggesting that the UV-induced isomerization can significantly inhibit AF adhesion and accumulation on the surface of the Azo-TbTh membrane (Figure 4c).

Prevention of the accumulated cake layer requires the membrane to rapidly repel the foulants after contact.[35–37] Therefore,

for the direct visualization of the improvement in fouling resistance, the Azo-TbTh membrane was challenged with the AF dye as the model pollutant. A droplet of AF dissolved in methanol was dropped on the membrane surface and then immersed into methanol to observe the adhesion behavior. As shown in Figure S13 and Movie S1 (Supporting Information), the majority of the AF droplet drifted away from the Azo-TbTh-*trans* membrane, while obvious red spots still can be detected on the membrane surface. In contrast, on the Azo-TbTh-*cis* membrane surface, instead of adhering to the membrane, the droplet quickly lifted and fully bounced away (Figure 4d; Movie S2, Supporting Information). This indicates that the Azo-TbTh-*cis* membrane can spontaneously recover its clean status in methanol, which could effectively isolate the membrane from the foulants.

In view of the strong methanol affinity of *cis*-azobenzene groups and the favorable self-cleaning ability of the Azo-TbTh-*cis* membrane, we expected the membrane to exhibit superior dynamic anti-fouling performance during periodic operations. Therefore, we tested time-dependent permeances by filtrating methanol and methanolic solutions alternately for three cycles (Figure 4e). The Azo-TbTh-*cis* membrane showed a stable methanol permeance of 57 L m^{-2} h^{-1} bar^{-1} after permeation for 60 min. The permeance was reduced to 40 L m^{-2} h^{-1} bar^{-1} when the feed was changed to the AF solution, which is mainly attributed to the accumulated AF molecules on the membrane surface. Notably, methanol cleaning could recover the permeance to 54 L m^{-2} h^{-1} bar^{-1}, giving a flux recovery ratio (*FRR*) of 96%. This indicates that the Azo-TbTh-*cis* membrane can further reduce the irreversible adsorption of dye molecules. During the following cyclic operations, the *FRR* of the Azo-TbTh-*cis* membrane remains unchanged, implying that dye adsorption approaches saturation in the first cycle. Moreover, the membrane basically sustains its initial morphology after this periodic operation (inset in Figure 4e). These results demonstrate that the Azo-TbTh-*cis* membrane maintains superior fouling resistance during long-term use.

2.4. Mechanism for the Antifouling Behavior

To understand the fouling resistance of the Azo-TbTh membrane upon UV exposure, quartz crystal microbalance (QCM) was utilized to monitor its real-time responses in the continuous flow of the AF solution. Briefly, the adsorption of AF molecules leads to significant resonance frequency change (Δf) of the QCM sensors, which reflects the antifouling ability of the Azo-TbTh membrane. In order to introduce the UV light into the chamber, the QCM was coupled with an ellipsometry module, thus in situ reflecting the Δf of the sensors under external UV exposure (Figure S14, Supporting Information).[38] Prior to QCM testing, the Azo-TbTh layer needs to be coated on the QCM chip. To this end, the QCM chip was alternatively soaked in the diluted precursor solutions to synthesize a thin layer of Azo-TbTh on the surface of the chip through the layer-by-layer strategy. An obvious decline in frequency is observed after switching methanol to the AF solution, which is ascribed to the adsorbed AF molecules (**Figure 5a**). After rinsing the surface with methanol, the sensor shows a frequency recovery ratio of ≈80%, indicating that the dye adsorption-desorption within the Azo-TbTh-trans layer is not completely reversible. Upon exposing the Azo-TbTh layer with 365 nm UV light for 40 min, the Δf was significantly decreased to 8 Hz from the initial 26 Hz for the Azo-TbTh-*trans* layer before UV exposure, reflecting that the adsorption of AF dyes on the Azo-TbTh-*cis* layer is 3 times lower than that of the Azo-TbTh-*trans* layer before UV exposure. More importantly, the frequency could basically recover to the initial value after methanol washing. This nearly complete recovery of the frequency demonstrates that the polar azobenzene groups can minimize the irreversible dye adsorption while the reversible adsorption can be easily removed by solvent washing. Furthermore, changes in solvent affinity within the trans-cis isomerization process were tracked during the continuous methanol flow. As shown in Figure 5b, the sensor undergoes a significant frequency decline under exposure to UV light, indicating that Azo-TbTh-*cis* could combine many more methanol molecules.

On the basis of the above structural analyses and QCM results, we elucidate a UV-light-enhanced antifouling mechanism for Azo-TbTh-*cis*. Azobenzene-branched nanochannels enable a controllable *trans-to-cis* isomerization upon UV exposure. The surface polarity is remarkably increased after the trans-to-cis transformation, leading to strengthened interactions between the membrane and polar solvents. In this situation, the polarized azobenzene groups can build a compact protective layer on the surface through the dipole-dipole interaction, effectively preventing the non-specific adsorption of foulants. The binding to foulants is energetically unfavorable owing to the free energy barrier which must be overcome to disturb the protective layer.

Motivated by the excellent fouling resistance, we sought to investigate the durability of the Azo-TbTh-*cis* membrane in the prolonged filtration test. As illustrated in Figure 5c, the membrane exhibits an unexpectedly stable OSN performance for 40-days continuous filtration. Furthermore, the membrane subjected to this long-term test remains intact without any damage or fouling spots (inset in Figure 5c). This demonstrates that the *trans-cis* photoisomerization strategy developed in this work can effectively enhance the fouling resistance of azobenzene-functionalized COF membranes in their long-term applications in OSN.

3. Conclusions

In summary, we propose a photo-induced strategy to synthesize highly permeable and durable nanofiltration membranes composed of polarity and pore size gradients along the COF pore channels. Azobenzene groups branched to the pore walls can be precisely remote-controlled by the UV light to trigger *trans-cis* isomerization, effectively enlarging the pore openings and simultaneously enhancing the polarity. As a result, the Azo-TbTh membrane in the *cis* state induced by UV exposure shows sharp molecular selectivity and exceptional solvent permeance. Also importantly, as a result of the well-established defense layer arising from tightly combined solvent molecules, the Azo-TbTh-*cis* membrane efficiently resists solute adhesion and the formation of the cake layer. These distinctive features make this membrane durable over a 40-day operation with negligible performance decline for its superior fouling resistance. We envision that the gradient structure conception by external photo induction would

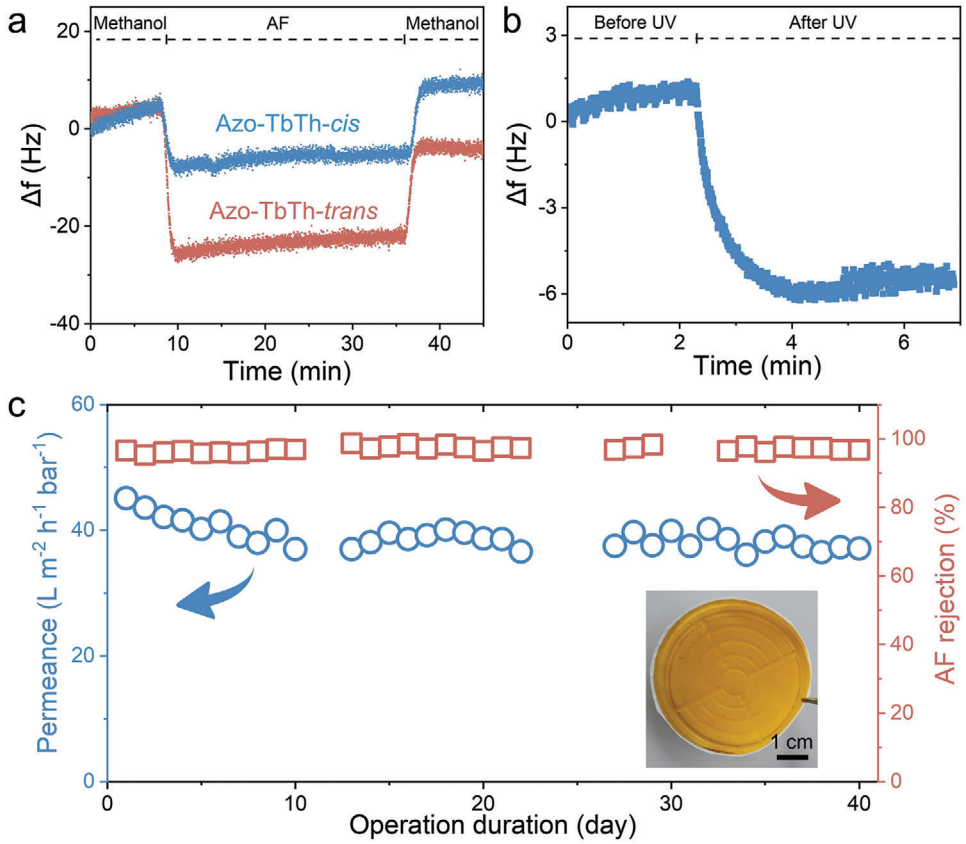

Figure 5. Analysis of the fouling resistance and durability of the Azo-TbTh-*cis* layer. a) Frequency changes of the Azo-TbTh-*trans* and Azo-TbTh-*cis* layer subjected to alternative immersion in methanol, methanolic solution of AF, and methanol. b) Frequency changes of the Azo-TbTh-*cis* layer in methanol upon UV exposure. c) Long-term OSN performance of the Azo-TbTh-*cis* membrane at the operation pressure of 1 bar. Inset is the photograph of the Azo-TbTh-*cis* membrane after continuous filtration for 40 days.

motivate the precise design and regulation of framework materials for diverse applications.

Supporting Information

Supporting Information is available from the Wiley Online Library or from the author.

Acknowledgements

This work was financially supported by the National Key Research and Development Program of China (2022YFB3805201) and the National Natural Science Foundation of China (22308147, 21825803). C.C.Y. is also grateful to the National Funding Program for Postdoctoral Talent (GZB20230135), China Postdoctoral Science Foundation (2023M740596) and Jiangsu Funding Program for Excellent Postdoctoral Talent (2023ZB679).

Conflict of Interest

The authors declare no conflict of interest.

Data Availability Statement

The data that support the findings of this study are available from the corresponding author upon reasonable request.

Keywords

antifouling, covalent organic frameworks, gradient structure, molecular separation, photoisomerization

Received: October 16, 2023
Revised: December 20, 2023
Published online:

[1] F. A. Jerca, V. V. Jerca, R. Hoogenboom, *Nat. Rev. Chem.* **2021**, *6*, 51.
[2] Z.-B. Zhou, P.-J. Tian, J. Yao, Y. Lu, Q.-Y. Qi, X. Zhao, *Nat. Commun.* **2022**, *13*, 2180.
[3] A. A. Beharry, G. A. Woolley, *Chem. Soc. Rev.* **2011**, *40*, 4422.
[4] A. Knebel, L. Sundermann, A. Mohmeyer, I. Strauß, S. Friebe, P. Behrens, J. Caro, *Chem. Mater.* **2017**, *29*, 3111.
[5] F. D. Jochum, P. Theato, *Chem. Soc. Rev.* **2013**, *42*, 7468.
[6] M. Fujiwara, T. Imura, *ACS Nano* **2015**, *9*, 5705.
[7] Y. Jiang, P. Tan, S.-C. Qi, X.-Q. Liu, J.-H. Yan, F. Fan, L.-B. Sun, *Angew. Chem., Int. Ed.* **2019**, *58*, 6600.
[8] Z. Wu, C. Ji, X. Zhao, Y. Han, K. Müllen, K. Pan, M. Yin, *J. Am. Chem. Soc.* **2019**, *141*, 7385.
[9] Y. Zhu, W. Zhang, *Chem. Sci.* **2014**, *5*, 4957.
[10] R. Huang, M. R. Hill, R. Babarao, N. V. Medhekar, *J. Phys. Chem. C* **2016**, *120*, 16658.

[11] J. Park, D. Yuan, K. T. Pham, J.-R. Li, A. Yakovenko, H.-C. Zhou, *J. Am. Chem. Soc.* **2012**, *134*, 99.
[12] S. Zhang, B. Gui, T. Ben, S. Qiu, *J. Mater. Chem. A* **2020**, *8*, 19984.
[13] Z. Wang, A. Knebel, S. Grosjean, D. Wagner, S. Brase, C. Woll, J. Caro, L. Heinke, *Nat. Commun.* **2016**, *7*, 13872.
[14] Liu, D. R. Dunphy, P. Atanassov, S. D. Bunge, Z. Chen, G. P. López, T. J. Boyle, C. J. Brinker, *Nano Lett.* **2004**, *4*, 551.
[15] T. Qian, H. Zhang, X. Li, J. Hou, C. Zhao, Q. Gu, H. Wang, *Angew. Chem., Int. Ed.* **2020**, *59*, 13051.
[16] Z. Wang, L. Heinke, J. Jelic, M. Cakici, M. Dommaschk, R. J. Maurer, H. Oberhofer, S. Grosjean, R. Herges, S. Bräse, K. Reuter, C. Wöll, *Phys. Chem. Chem. Phys.* **2015**, *17*, 14582.
[17] X. Guo, T. Mao, Z. Wang, P. Cheng, Y. Chen, S. Ma, Z. Zhang, *ACS Cent. Sci.* **2020**, *6*, 787.
[18] N. Huang, X. Ding, J. Kim, H. Ihee, D. Jiang, *Angew. Chem., Int. Ed.* **2015**, *54*, 8704.
[19] F. Yu, W. Liu, B. Li, D. Tian, J.-L. Zuo, Q. Zhang, *Angew. Chem., Int. Ed.* **2019**, *58*, 16101.
[20] N. Huang, L. Zhai, H. Xu, D. Jiang, *J. Am. Chem. Soc.* **2017**, *139*, 2428.
[21] Z. Li, T. He, Y. Gong, D. Jiang, *Acc. Chem. Res.* **2020**, *53*, 1672.
[22] J. Yuan, X. You, N. A. Khan, R. Li, R. Zhang, J. Shen, L. Cao, M. Long, Y. Liu, Z. Xu, H. Wu, Z. Jiang, *Nat. Commun.* **2022**, *13*, 3826.
[23] J. Zhang, L. Wang, N. Li, J. Liu, W. Zhang, Z. Zhang, N. Zhou, X. Zhu, *CrystEngComm* **2014**, *16*, 6547.
[24] G. Das, T. Prakasam, M. A. Addicoat, S. K. Sharma, F. Ravaux, R. Mathew, M. Baias, R. Jagannathan, M. A. Olson, A. Trabolsi, *J. Am. Chem. Soc.* **2019**, *141*, 19078.
[25] J. Liu, S. Wang, T. Huang, P. Manchanda, E. Abou-Hamad, S. P. Nunes, *Sci. Adv.* **2020**, *6*, eabb3188.
[26] C. Yin, Z. Zhang, Z. Si, X. Shi, Y. Wang, *Chem. Mater.* **2022**, *34*, 9212.
[27] L. Guo, Y. Yang, F. Xu, Q. Lan, M. Wei, Y. Wang, *Chem. Sci.* **2019**, *10*, 2093.
[28] S. Zhao, C. Jiang, J. Fan, S. Hong, P. Mei, R. Yao, Y. Liu, S. Zhang, H. Li, H. Zhang, C. Sun, Z. Guo, P. Shao, Y. Zhu, J. Zhang, L. Guo, Y. Ma, J. Zhang, X. Feng, F. Wang, H. Wu, B. Wang, *Nat. Mater.* **2021**, *20*, 1551.
[29] Z. Mu, Y. Zhu, B. Li, A. Dong, B. Wang, X. Feng, *J. Am. Chem. Soc.* **2022**, *144*, 5145.
[30] J. Yao, C. Liu, X. Liu, J. Guo, S. Zhang, J. Zheng, S. Li, *J. Membr. Sci.* **2020**, *601*, 117864.
[31] M. Han, D. Ishikawa, T. Honda, E. Ito, M. Hara, *Chem. Commun.* **2010**, *46*, 3598.
[32] L. Nie, K. Goh, Y. Wang, J. Lee, Y. Huang, H. E. Karahan, K. Zhou, M. D. Guiver, T.-H. Bae, *Sci. Adv.* **2020**, *6*, eaaz9184.
[33] A. He, Z. Jiang, Y. Wu, H. Hussain, J. Rawle, M. E. Briggs, M. A. Little, A. G. Livingston, A. I. Cooper, *Nat. Mater.* **2022**, *21*, 463.
[34] B. Sengupta, Q. Dong, R. Khadka, D. K. Behera, R. Yang, J. Liu, J. Jiang, P. Keblinski, G. Belfort, M. Yu, *Science* **2023**, *381*, 1098.
[35] H. Li, J. Zhang, S. Gan, X. Liu, L. Zhu, F. Xia, X. Luo, Q. Xue, *Adv. Funct. Mater.* **2023**, *33*, 2212582.
[36] D. Dong, Y. Zhu, W. Fang, M. Ji, A. Wang, S. Gao, H. Lin, R. Huang, J. Jin, *Adv. Funct. Mater.* **2022**, *32*, 2113247.
[37] D. H. Seo, S. Pineda, Y. C. Woo, M. Xie, A. T. Murdock, E. Y. M. Ang, Y. Jiao, M. J. Park, S. I.l Lim, M. Lawn, F. F. Borghi, Z. J. Han, S. Gray, G. Millar, A. Du, H. K. Shon, T. Y. Ng, K. Ostrikov, *Nat. Commun.* **2018**, *9*, 683.
[38] X. Zhou, Z. Wang, R. Epsztein, C. Zhan, W. Li, J. D. Fortner, T. A. Pham, J.-H. Kim, M. Elimelech, *Sci. Adv.* **2020**, *6*, eabd9045.